Thermal Stability of Silica for Application in Thermal Energy Storage

Preprint

Patrick Davenport[1], Zhiwen Ma[1], William Nation[2], Jason Schirck[2], Aaron Morris[2], and Matthew Lambert[3]

1 National Renewable Energy Laboratory
2 Purdue University
3 Allied Mineral Products

Presented at the 26th SolarPACES Conference 2020
September 28 – October 2, 2020

NREL is a national laboratory of the U.S. Department of Energy
Office of Energy Efficiency & Renewable Energy
Operated by the Alliance for Sustainable Energy, LLC

This report is available at no cost from the National Renewable Energy Laboratory (NREL) at www.nrel.gov/publications.

Contract No. DE-AC36-08GO28308

Conference Paper
NREL/CP-5700-77426
October 2020

Thermal Stability of Silica for Application in Thermal Energy Storage

Preprint

Patrick Davenport[1], Zhiwen Ma[1], William Nation[2], Jason Schirck[2], Aaron Morris[2], and Matthew Lambert[3]

1 National Renewable Energy Laboratory
2 Purdue University
3 Allied Mineral Products

Suggested Citation
Davenport, Patrick, Zhiwen Ma, William Nation, Jason Schirck, Aaron Morris, and Matthew Lambert. 2020. *Thermal Stability of Silica for Application in Thermal Energy Storage: Preprint*. Golden, CO: National Renewable Energy Laboratory. NREL/CP-5700-77426. https://www.nrel.gov/docs/fy21osti/77426.pdf.

NREL is a national laboratory of the U.S. Department of Energy
Office of Energy Efficiency & Renewable Energy
Operated by the Alliance for Sustainable Energy, LLC

This report is available at no cost from the National Renewable Energy Laboratory (NREL) at www.nrel.gov/publications.

Contract No. DE-AC36-08GO28308

Conference Paper
NREL/CP-5700-77426
October 2020

National Renewable Energy Laboratory
15013 Denver West Parkway
Golden, CO 80401
303-275-3000 • www.nrel.gov

NOTICE

This work was authored in part by the National Renewable Energy Laboratory, operated by Alliance for Sustainable Energy, LLC, for the U.S. Department of Energy (DOE) under Contract No. DE-AC36-08GO28308. Funding provided by U.S. Department of Energy Advanced Research Projects Agency – Energy (ARPA-E), as well as Gen3 CSP under DOE's Office of Energy Efficiency and Renewable Energy (EERE), Solar Energy Technologies Office (SETO). The views expressed herein do not necessarily represent the views of the DOE or the U.S. Government.

Cover Photos by Dennis Schroeder: (clockwise, left to right) NREL 51934, NREL 45897, NREL 42160, NREL 45891, NREL 48097, NREL 46526.

Thermal Stability of Silica for Application in Thermal Energy Storage

Patrick Davenport[1,a)], Zhiwen Ma[1], William Nation[2], Jason Schirck[2], Aaron Morris[2], and Matthew Lambert[3]

[1] *National Renewable Energy Laboratory, 15013 Denver West Parkway, Golden, CO 80401, USA.*
[2] *School of Mechanical Engineering, Purdue University, West Lafayette, IN 47907, USA.*
[3] *Allied Mineral Products, 2700 Scioto Parkway, Columbus, OH 43221, USA.*

[a)] Corresponding author: Patrick.Davenport@nrel.gov

Abstract. Thermal energy storage (TES) systems have enabled concentrating solar power (CSP) to remain competitive in the modern energy mix by providing economical load shifting grid services and firming up intermittent solar resource. Free from siting constraints, TES also shows promise as an economical alternative to traditional pumped-storage hydropower (PSH) and compressed air energy storage (CAES). As potential thermal energy storage media, some solid particles demonstrate stability over wide temperature ranges which allows for increased sensible energy storage density and is essential in achieving low-cost storage. Silica sand, in the form of α-quartz, is one such candidate. This work presents a brief review of relevant silica thermophysical properties and further investigates the thermal stability of silica particles as a candidate TES media by subjecting them to two different thermal tests: (1) a 500-hour thermal treatment at 1200°C under varied atmospheres; and (2) cycling 25, 50, and 100 times between 300°C and 1200°C. For both tests, particle stability is examined by means of pre- and post-treatment Mie scattering. An additional XRD analysis is conducted for the 500-hour treatment in air. Results indicate limited changes in both particle distribution and crystallographic structure which is promising for the application as solid particle media for thermal energy storage.

MOTIVATION

Advances in grid-scale, long duration energy storage technologies are necessary to support continued grid integration of renewable energy resources. Traditional pumped-storage hydropower (PSH) installations are limited by geographic opportunity, and compressed air energy storage (CAES) is constrained by existing geologic sites. Demonstrated by commercial concentrating solar power (CSP) plants, thermal energy storage (TES) shows promise as an economical alternative that is free from siting constraints if operated as a stand-alone system [1,2].

Historically, particle-based CSP efforts have focused on aluminosilicate particles produced by CARBO Ceramics Inc. because the particles have a high solar-weighted absorptivity that supports current direct-absorption falling particle receiver designs [3]. In the case of a stand-alone TES system, particle selection is no longer governed by radiative properties, but rather, by particle stability, flowability, availability, and achievable energy density. Operating under this new paradigm, the authors were motivated to investigate the suitability of silica sand for application alongside CSP systems and as a stand-alone, scalable, low cost TES system under development at the National Renewable Energy Laboratory [4].

In the stand-alone TES system [5], *charging* is achieved by heating inexpensive solid particles (e.g. silica sand) using off-peak, low-price electricity. The particles are stored for 10-100 hours in highly-effective insulated hot silos [6]. During peak hours, energy *discharging* is achieved by gravity feeding the hot particles through a fluidized-bed heat exchanger to transfer particle heat to a thermal power system (e.g. conventional steam-Rankine, air Brayton turbine with combined-cycle ability, or emerging sCO2 Brayton power cycle).

This work presents a brief review of relevant silica thermophysical properties and further investigates the thermal stability of silica particles as a candidate TES media by subjecting them to two different thermal tests: (1) a 500-hour

thermal treatment at 1200°C under varied atmospheres; and (2) cycling 25, 50, and 100 times between 300°C and 1200°C. The varied atmospheres capture potential power system working fluid conditions (e.g. air, nitrogen, or humidified air in case steam-injection is utilized). For both tests, particle stability is examined by means of pre- and post-treatment Mie scattering. An additional XRD analysis is conducted for the 500-hour treatment in air.

BACKGROUND

Abundance: The bulk of round, ultra-pure (>99.0%) silica sand in the United States exists in the form of fine- to medium-grained (80-2000um) particles, and is deposited in St. Peter's Sandstone which spans across the Midwest as shown in Fig. 1. In Missouri, the formation averages 25-30 meters thick and bears an estimated 3.4 trillion tons of well-sorted, friable silica, most of which is accessed directly from the face of quarries before being washed, dried, and sieved into desired distributions [7]. Originally sourced for glass manufacture, St. Peter's silica has since been adopted into markets as a paint additive, filler material, polishing compound, filtering media, and more recently as a fracture proppant due in part to abundance and low cost ($30-50/ton).

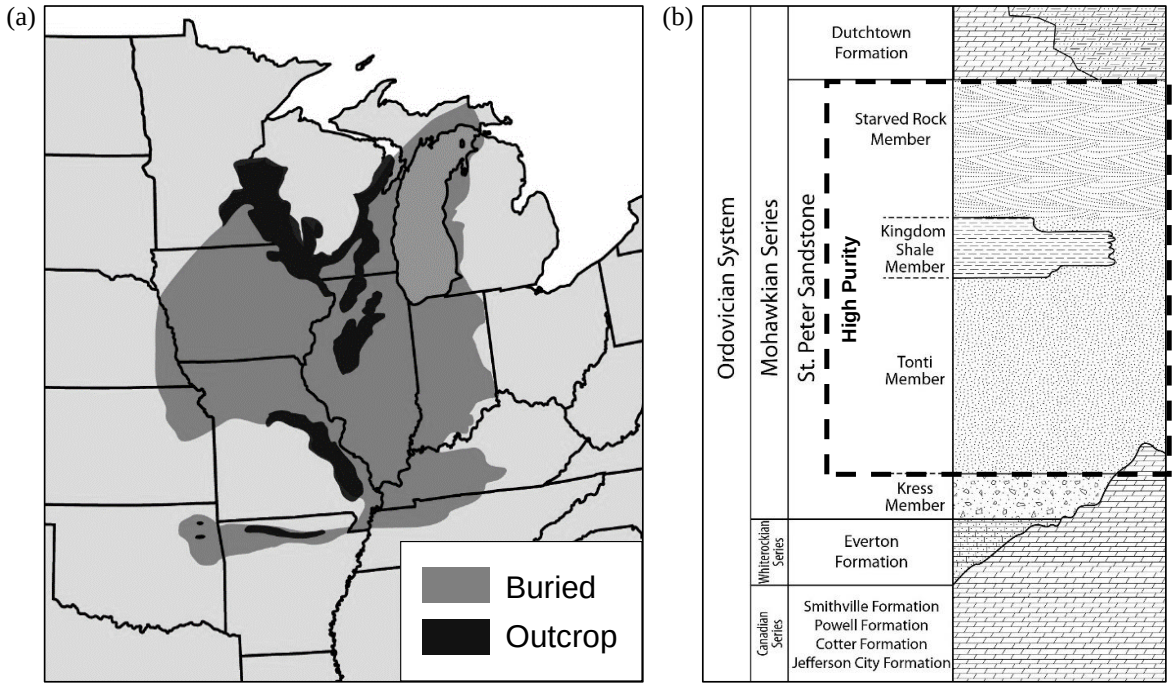

FIGURE 1. Distribution of St. Peter's Sandstone deposit (a) and illustrative geologic column of the deposit's high-purity zone and bounding units (b), reproduced with permission from Davis [7].

Structure: Silica (SiO2) is comprised of elemental silicon and oxygen: the two most abundant elements found in Earth's crust [8]. At the atomic level, covalent hybridization of the silicon anion's *3s* and *3p* orbitals support bond angles ranging from 120-180 degrees which allows for an array of potential SiO_4^{4-} tetrahedral structures [9]. Although 13-25 silica polymorphs have been identified [10–12], the bulk of silica at Earth's surface is stable in the form of low-temperature α-quartz with traces of α-tridymite and α-cristobalite present when an insufficient amount of time was afforded during natural formation for 100% conversion to quartz.

Quartz Inversion: When heated at ambient pressure, low-temperature α-quartz is stable up to 573°C, at which point it undergoes a *displacive* transformation to high-temperature β-quartz [12]. Unlike *reconstructive* transformations, which involve breaking bonds, require more energy, and occur over a long period of time, *displacive* transformations occur at a defined temperature, and are relatively rapid and reversible as they involve only slight alteration of bond angles within the lattice [13]. The speed of this "quartz inversion" was described in 1928 as: "very high [and that] all attempts to check the reaction, once it had started, were futile" [14]. The unit cells and c-axis projections shown in Fig. 2 illustrate the inversion from α-quartz to β-quartz [15].

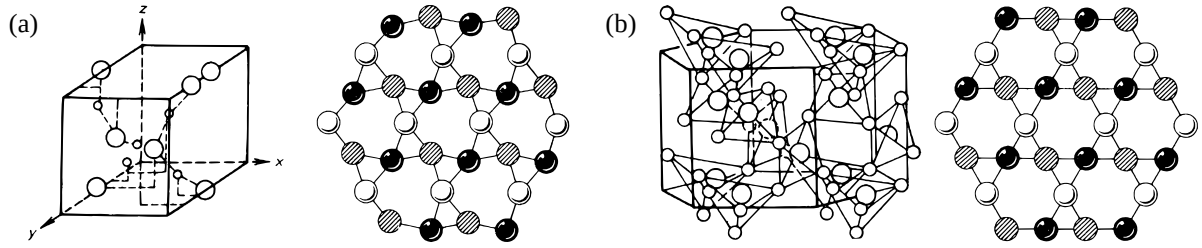

FIGURE 2. Crystallographic unit cells and c-axis projections for (a) rhombohedral (or trigonal) low-temperature α-quartz and (b) hexagonal high-temperature β-quartz. Reprinted from *Silica Glass and its Application*, 1st edition, I. Fanderlik, Copyright 1991, with permission from Elsevier [15].

Heat Capacity: From ambient temperature to 1200°C, the heat capacity of quartz ranges from approximately 750 to 1200 J/kg·°C, though published data varies depending on sample type and treatment of the quartz inversion [16]. To complicate matters more, the thermodynamic property changes induced by the quartz inversion differ depending on the origin and size fraction of the sample: in general, large particles favor the spontaneous formation the α-phase, whereas small particles stabilize the β-phase [17]. Such variations are captured in Fig. 3, which shows heat capacity of quartz over 300-1200°C from two different data sources.

Enthalpy of Transformation: Ghiorso et al. present published transformation enthalpies ($\Delta H_{\alpha\text{-}\beta}$) for quartz ranging from 80-290 cal/mol (5.57-20.19 J/g), alongside their own results obtained from DSC runs over a 9.0°C interval [18]. In agreement with other accounts, Ghiorso et al. find $\Delta H_{\alpha\text{-}\beta}$ to be dependent upon sample grain size, with $\Delta H_{\alpha\text{-}\beta}$ = 92.0 ±1.4 cal/mol (6.41 J/g, ~Δ5.5°C equivalent) for crushed powder, and $\Delta H_{\alpha\text{-}\beta}$ = 107.7±1.4 cal/mol (7.45 J/g, ~Δ6.3°C equivalent) for a single piece of quartz. The volumetric change associated with the transformation is reported at 1.6% [19], which can lead to failures if heating in a vessel under stationary conditions.

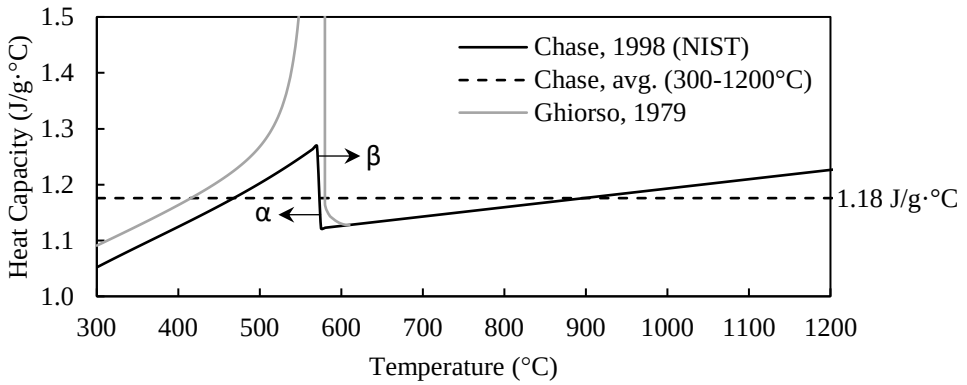

FIGURE 3. Heat capacity of quartz over 300-1200°C including the α-β inversion at 573°C [16,18].

Melting: The detailed response of β-quartz to further heating is unresolved, but reportedly depends on heating rate: when heated quickly, it can exist in a metastable state up to 1,470°C before melting at ~1550°C [20]; when heated gradually, a transition to β-cristobalite is thought to take place by a metastable inversion at lower temperatures (>1150°C) [12] or (>1200°C) [21] before eventually melting at ~1713°C [22]. The transition from β-quartz to β-cristobalite is unclear due to the sluggish, reconstructive kinetics, and can be influenced by the further presence of impurities. While ultra-pure silica from St. Peter's Sandstone is expected to follow these observations, research from fluidized bed combustion and gasification processes demonstrate that the presence of sufficient alkali metals (particularly potassium) leads to lower temperature necking and eventual agglomeration of particles by weak bridging [23–25] which may impact performance for less pure sand sources.

METHODOLOGY

This work investigates two distributions of *Northern White* silica particles, previously known as *Wedron*, that were sourced from St. Peter's Sandstone in Illinois by the Covia Corporation. Figure 4 shows an example of the sample size used for the 500-hour experimental tests, particles viewed under an optical microscope, and the particle chemical composition. Figure 5 shows the two baseline particle distributions, silica 430 and silica 460.

(a)

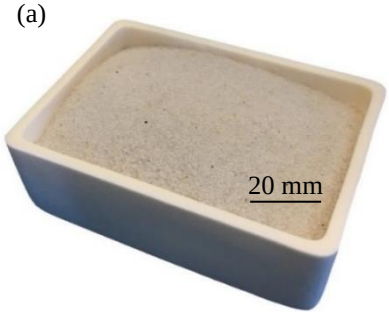

(b)

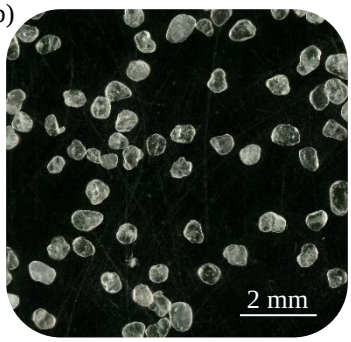

(c)

Chemical Composition	
SiO_2	99.65%
Al_2O_3	0.065%
Fe_2O_3	0.018%
TiO_2	0.011%
CaO	0.012%
Other	0.244%

FIGURE 4. A 120 ml alumina raft used in 500-hour tests (a); example of particle morphology under an optical microscope (b); and silica chemical composition (c).

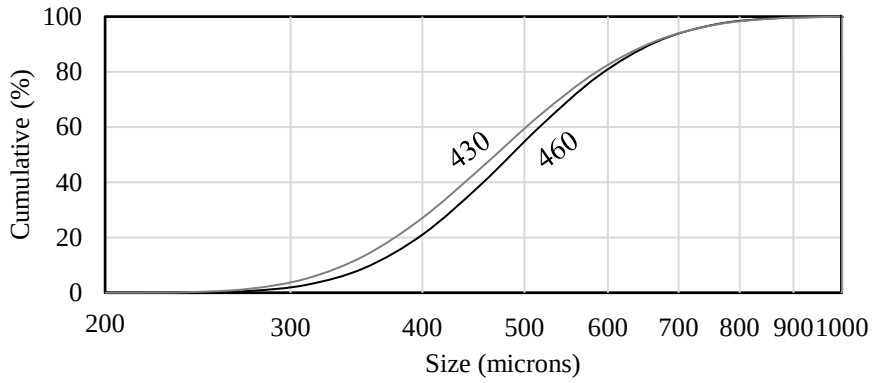

FIGURE 5. Baseline "as-received" particle distributions for *Northern White* silica sand 430 and 460.

The following paragraphs describe the two thermal tests: (1) a 500-hour thermal treatment of silica 460 at 1200°C under varied atmospheres; and (2) cycling of silica 430 and silica 460 for 25, 50, and 100 cycles between 300°C and 1200°C. The characterization techniques used to evaluate particle stability are also briefly described.

500-hour Thermal Stability Test

Three 500-hour thermal treatments were performed to investigate silica 460 stability at 1,200°C under different atmospheres: air, humidified air (pH_2O=50%), and nitrogen. The tests were conducted in a Lindberg/Blue M™ box furnace equipped with a gas inlet. The furnace was ramped to 1,200°C (10°C/min), held for 500 hours, and left to cool to ambient temperature at its natural cooling rate. In each case, the respective cover gas was supplied at a rate of 400 sccm to refresh the furnace volume approximately every 15 minutes. The experimental setup used to supply the furnace with 50% partial pressure steam is shown in Fig. 6.

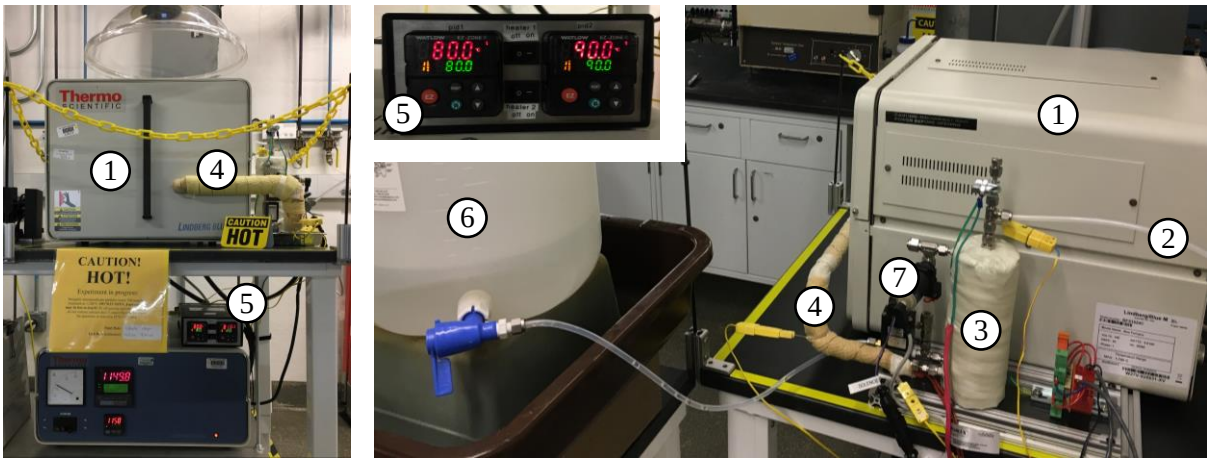

FIGURE 6. Experimental setup used to purge a Lindberg/Blue M™ box furnace (1) with humidified air (pH_2O=50%) for 500 hours. Supply gas (2) is bubbled through a humidifier (3) at a rate of 400 sccm. The humidifier and subsequent delivery line (4) are maintained by PID controllers (5) at 80°C and 90°C, respectively, to prevent condensation. A DI water reservoir (6) maintains the humidifier via a solenoid valve actuated by an optical water-level sensor (7). Humidified air (pH_2O=50%) is confirmed by an in-line Vaisala™ humidity meter (Series HMT330). Photos used with permission by Patrick Davenport.

Thermal Cycling Test

An additional thermal treatment was performed to investigate silica 430 and 460 stability in response to repeated cycling between 300 and 1,200°C. The cycling was conducted in a SentroTech box furnace with air as a cover gas. The furnace was ramped between 300°C and 1,200°C (5°C/min) with a 1-hour dwell period at both extremes. Samples were removed and analyzed after 25, 50, and 100 cycles.

Particle Stability Characterization

Subsamples of "as-received" particles were obtained from the bulk shipment using a perforated core sampling tube, a common industrial quality assurance practice that helps mitigate the influence of particle segregation during filling and transport. For both tests, changes in particle distribution pre- and post-treatment were characterized by Mie scattering using a Malvern Mastersizer 3000. In conducting the analyses, a particle refractive index of 1.457 and absorptive index of 0.01 were assigned according to the Malvern library for SiO_2, and air was used for particle dispersion. For the 500-hour treatment in air, pre- and post-treatment powder x-ray diffraction was conducted at 1°/min on silica 460 using a Rigaku DMax.

RESULTS AND DISCUSSION

Response to Thermal Stability Test

Figures 7-9 show the particle distribution shifts relative to the silica 460 baseline following the three treatments. The pre- and post-treatment curves were each determined using 13-15 measurements with ±1σ indicated by dotted curves. The respective deviation of the median particle diameter by volume (D_v50) for treatment under air, nitrogen, and humidified air are -2.46%, -1.38%, and -2.61%, respectively (red lines).

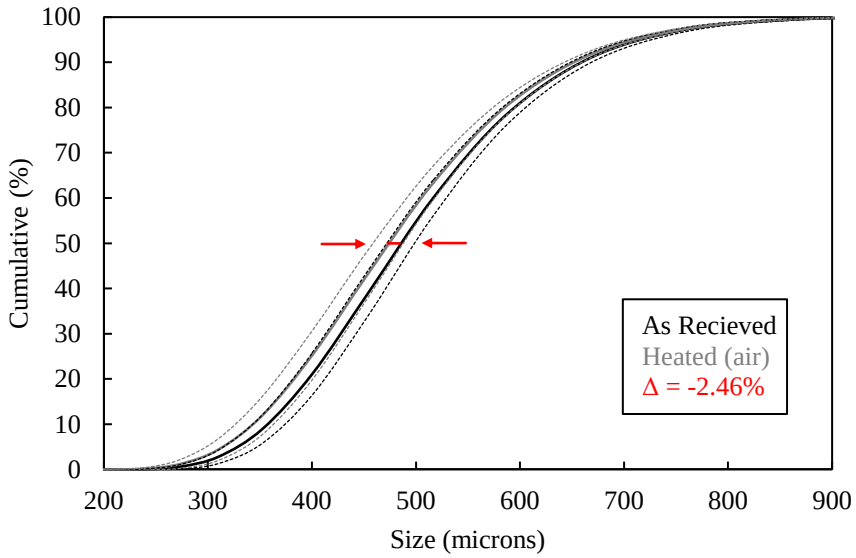

FIGURE 7. Silica 460 particle distribution shift (gray curve) after 500-hour thermal treatment in air at 1,200°C, relative to "as received" (black curve). A -2.46% shift in median particle diameter (D_v50) is observed and indicated by a red line.

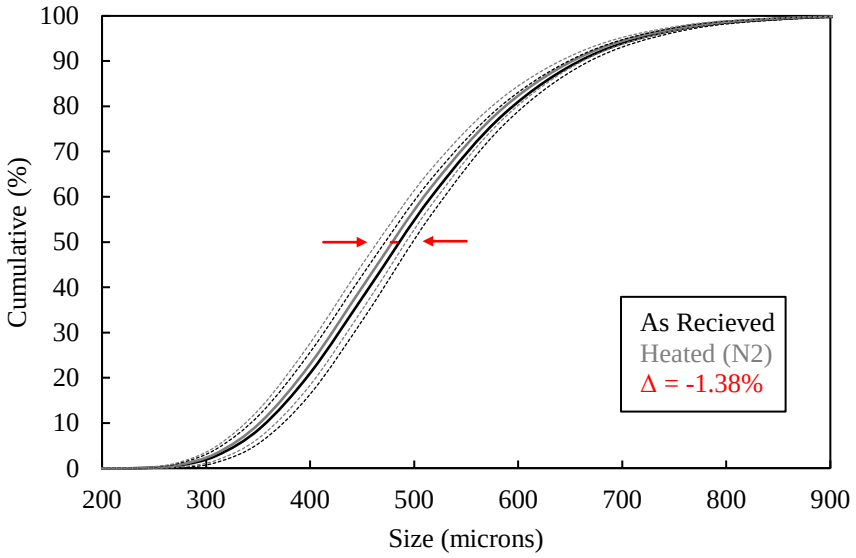

FIGURE 8. Silica 460 particle distribution shift (gray curve) after 500-hour thermal treatment in nitrogen at 1,200°C, relative to "as received" (black curve). A -1.38% shift in median particle diameter (D_v50) is observed and indicated by a red line.

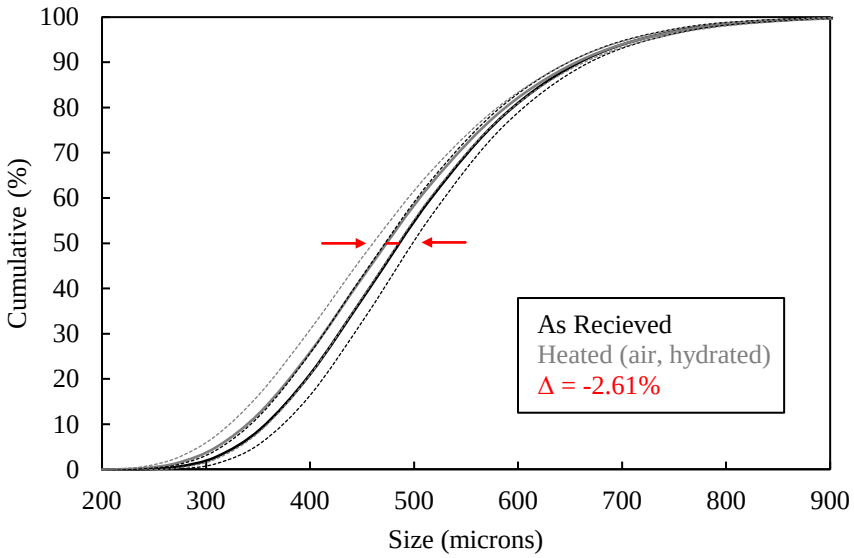

FIGURE 9. Silica 460 particle distribution shift (gray curve) after 500-hour thermal treatment in humidified air (pH2O=50%) at 1,200°C, relative to "as received" (black curve). A -2.61% shift in median particle diameter (D_v50) is observed and indicated by a red line.

An unpaired student's T-test indicates that the shifts observed under air and humidified atmospheres are statistically significant at the 95% confidence level, while the shift observed under nitrogen is not. The median particle diameter is derived from the *volume equivalent sphere* model and is selected as the figure of merit in this study because it is less sensitive to outliers than the average particle diameter, and thus, is more relevant to system economics.

Qualitatively, the particles showed no signs of agglomeration or sintering upon removal from the furnace in preparation for post-treatment analysis. Figure 10 shows a representative angle of repose (~25°) achieved after testing which was consistent across all samples. Considering the lack of change in overall distribution shape, the slight reduction in particle diameter across all tests may be an artifact of Mie scattering— a burn-out cycle was not performed to clean organic materials from the "as received" particle surfaces before establishing a baseline, and surface contaminants may influence the particle refractive/absorptive indices which are used as input for Mie scattering.

FIGURE 10. Example demonstrating particle angle of repose achieved after testing.

Response to Thermal Cycling Stability

Figure 11 and Figure 12 show the particle distribution shifts observed after 25, 50, and 100 cycles relative to the baseline. Unlike the 500-hour tests, sample size was reduced here in an effort to expedite the cycling rate. Consequently, each curve displayed represents the average of three measurements rather than 13-15 as in the 500-hour tests, so statistical evaluation is not preformed.

For silica 460, as cycles progress, particle diameter appears to decrease slightly, then increase again. Conversely, for silica 430, particle diameter appears to increase more dramatically, then decrease. These observations, where the mean particle diameter fluctuates within each experiment and the fluctuations oppose one another between

experiments, suggest that the observed changes in median particle diameter may result from analysis variability, too few samples, sampling process, or artifacts from sample handling. The largest observed shift is a 10.50% increase in particle diameter for Silica 430 following 50 cycles, but this decreases to 6.9% after 100 cycles, which indicates certain measurement uncertainties inducing some variance.

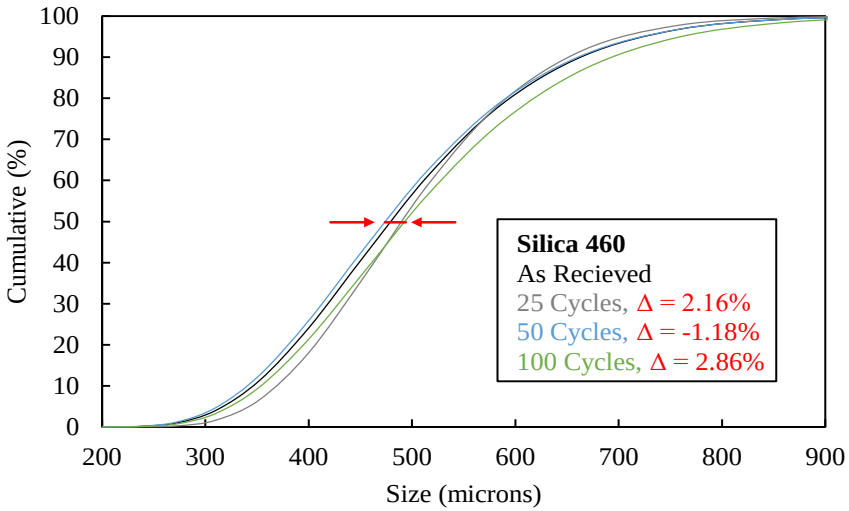

FIGURE 11. Particle distribution shifts after 25, 50, and 100 cycles relative to the baseline for Silica 460.

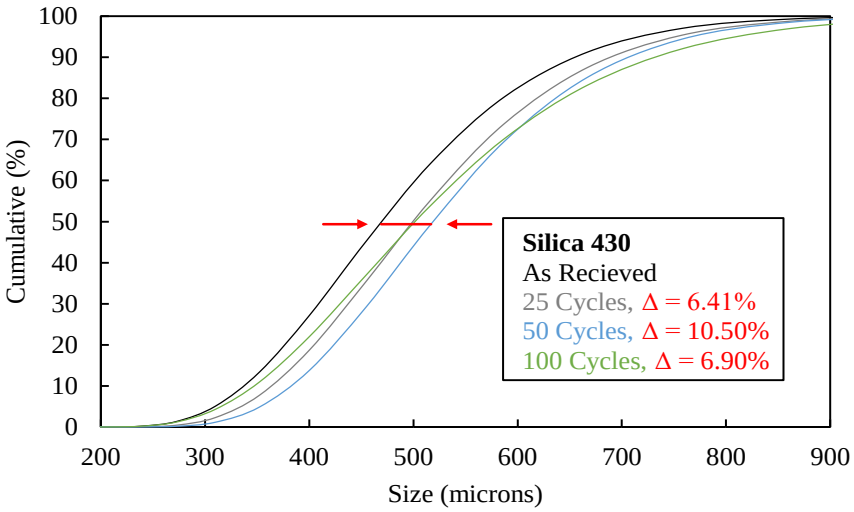

FIGURE 12. Particle distribution shifts after 25, 50, and 100 cycles relative to the baseline for Silica 430.

In order to better examine changes in particle distribution shape, all curves are translated to a common, relative median particle diameter in Figure 13. In practice, a widening particle distribution may be indicative of particle cleavage. For silica 460, as cycles progress, the particle distribution is shown to narrow, then widen slightly. For silica 430, the particle distribution remains relatively constant before widening. The lack of an obvious trend and relatively low magnitude of change in distribution shape suggests that the observed changes may result from analysis variability.

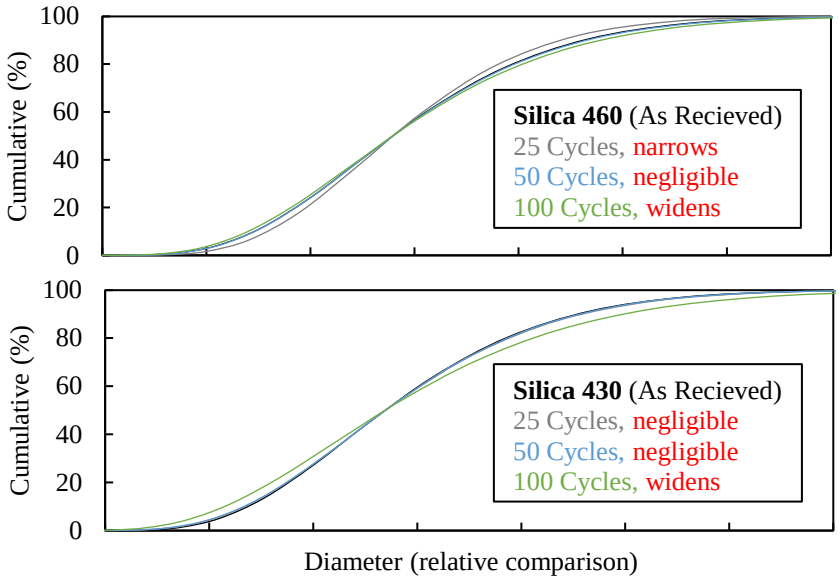

FIGURE 13. Particle distributions translated to a common, arbitrary median particle diameter for general shape comparison.

The authors recognize that these observations may appear to contradict prior work by the German Aerospace Center (DLR) where cleavage of quartz sand is evidenced by changes in particle distributions after 5, 10, and 30 cycles [26]. An attempt to corroborate differences is provided here.

At DLR, particles with a mean diameter of 800um were quenched from 810°C using 20°C water. In doing so, the process achieves a cooling rate of 3034°C/s which is ~54% of the theoretical maximum rate (5646°C/s) that the residual tensile stress at the surface of quartz particles of that size can withstand. The current study differs in a few respects: (1) the cooling rate is orders of magnitude lower than that applied at DLR, leaving a greater margin to accommodate stress concentrations that occur across non-spherical particles and at surface defects; and (2) the particles in this study are highly spherical, and monocrystalline in nature— some quartz deposits are comprised of polycrystalline quartz which would be accompanied by preferred intergranular cleavage (although source and crystalline nature of DLR particles is undisclosed).

XRD Analysis

XRD spectra was taken for silica 460 before and after the 500-hour test in air. Figure 14 compares: (a) the "as received" spectra to a calculated theoretical powder diffraction file (PDF) for α-quartz, confirming that the sample is composed of high-purity α-quartz; (b) the "as received" and "heated" spectra, showing a sign of peak development at $2\theta = 21.94°$; and (c) the "heated" spectra and calculated theoretical α-cristobalite PDF, confirming that the peak development at $2\theta = 21.94°$, 28.37°, and 31.35° corresponds to α-cristobalite spacing of the 101, 111, and 102 crystallographic planes, respectively.

Further spectral analysis indicates that the "as received" sample constituents resemble: α-quartz (64.8%), β-quartz (18.1%), α-cristobalite (9.7%), and tridymite (7.4%). After 500-hours at 1,200°C in air, the "heated" sample constituents resemble: α-quartz (47.0%), β-quartz (30.3%), α-cristobalite (17.1%), and tridymite (5.6%). It should be noted that spectral analysis and the associated percentages are highly subjective, depending on consistent sample preparation, machine operation and accuracy, and additional decisions made by the analyzer. Due to this and the relatively fast scan rate (1°/min), values presented here should be scrutinized relative to one another.

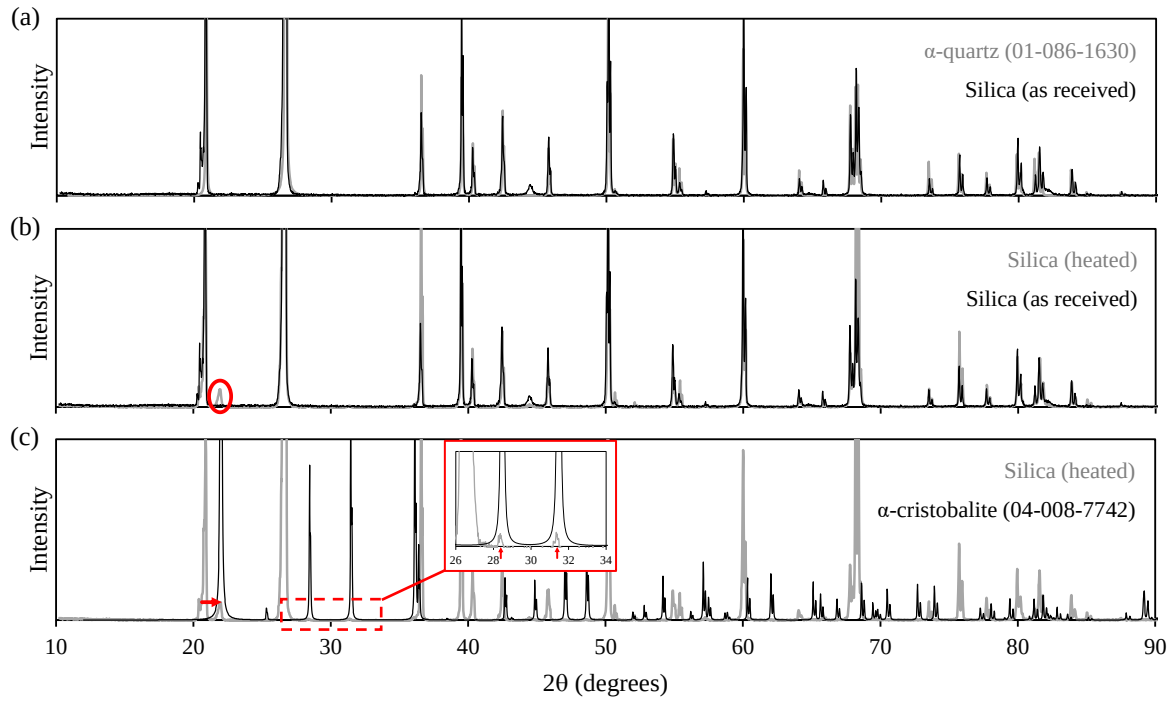

FIGURE 14. (a) Overlay of "as received" XRD spectra and theoretically calculated α-quartz PDF (01-086-1630) confirms that sample is composed of high-purity α-quartz; (b) overlay of "as received" and "heated" spectra show sign of peak development at a 2θ = 21.94°, 28.37°, and 31.35°; (c) overlay of "heated" spectra and theoretically calculated α-cristobalite PDF (04-008-7742) indicates some degree of cristobalite formation.

CONCLUSIONS

Following a brief review of relevant silica thermophysical properties, the thermal stability of silica particles as a candidate media for thermal energy storage was investigated by subjecting them to two different thermal tests: (1) a 500-hour thermal treatment at 1200°C under varied atmospheres; and (2) cycling 25, 50, and 100 times between 300°C and 1200°C.

For the 500-hour test, limited statistically significant changes in the mean particle diameter are observed for treatment under air and hydrated air, but not under nitrogen. All changes remain below 3% compared to the "as received" particles. Future testing may include a preliminary burn-out cycle to clean organic materials from the "as received" particle surfaces before generating a baseline since surface contaminants may influence the particle refractive and absorptive indices which are used as input to perform Mie scattering.

For the thermal cycling test, the largest observed shift in median particle diameter is a 10.50% increase following 50 cycles. This and the other observed shifts are attributed to analysis variability due to an insufficient sample size or sampling. Future testing will focus on obtaining more robust data so that statistical significance can be determined. Additionally, application of more aggressive cycling test ramp rates that reflect specific TES system needs may provide field-use indications.

XRD analysis confirms the high-purity nature of the sourced α-quartz. Peak development at 2θ = 21.94°, 28.37°, and 31.35° indicates the development (or inclusion of) a small degree of α-cristobalite (spectral analysis indicates a relative increase of 7.4% after heating). Because samples were not covered inside the furnace, particles at the surface of the crucibles were exposed to severe infrared radiation and may have reached temperatures well over 1,200°C which could drive α-cristobalite formation. Future thermal testing could shield particles from such exposure, and XRD could be performed with a slower scan rate for improved resolution.

These results, indicating limited changes in both particle distribution and crystallographic structure, combined with the overall abundance and low cost of high-purity silica sand, demonstrate its promise as a solid particle media for economic thermal energy storage systems.

ACKNOWLEDGMENTS

This work was authored by the National Renewable Energy Laboratory (NREL), operated by Alliance for Sustainable Energy, LLC, for the U.S. Department of Energy (DOE) under Contract No. DE-AC36-08GO28308. The authors gratefully acknowledge support from the U.S. Department of Energy Advanced Research Projects Agency – Energy (ARPA-E), as well as Gen3 CSP under the U.S. DOE, Office of Energy Efficiency and Renewable Energy (EERE), Solar Energy Technologies Office (SETO).

The authors thank Dr. Matt Yung (NREL) for not only providing access to, but also allowing modification of the Lindberg/Blue M™ box furnace used in the 500-hour tests. The authors also thank Dr. David Albin and Dr. Sam Gage for providing guidance and insight regarding XRD best practices.

REFERENCES

1. Z. Ma, G. C. Glatzmaier, and C. F. Kutscher, "The Thermal Energy Storage Solution," Sol. Today **26** (2012), pp. 22–26.
2. M. Mehos, C. Turchi, J. Vidal, M. Wagner, Z. Ma, C. Ho, W. Kolb, C. Andraka, Z. Ma, A. Kruizenga, and NREL, *Concentrating Solar Power Gen3 Demonstration Roadmap* (2017).
3. N. P. Siegel, M. D. Gross, and R. Coury, "The Development of Direct Absorption and Storage Media for Falling Particle Solar Central Receivers," J. Sol. Energy Eng. Trans. ASME **137** (2015), pp. 1–7.
4. Advanced Research Projects Agency – Energy (ARPA-E), "Economic Long-Duration Electricity Storage by Using Low-Cost Thermal Energy Storage and High-Efficiency Power Cycle." (2018) [Online]. Available: https://arpa-e.energy.gov/?q=slick-sheet-project/economic-long-duration-electricity-storage-using-low-cost-thermal-energy-storage.
5. Z. Ma, P. Davenport, and R. Zhang, "Design Analysis of a Particle-Based Thermal Energy Storage System for Concentrating Solar Power or Grid Energy Storage," J. Energy Storage **29** (2020), p. 101382.
6. J. Gifford, Z. Ma, and P. Davenport, "Thermal Analysis of Insulation Design for a Thermal Energy Storage Silo Containment for Long-Duration Electricity Storage," Front. Energy Res. **8** (2020), pp. 1–12.
7. J. G. Davis, "St. Peter Sandstone Mineral Resource Evaluation, Missouri, USA," Proc. 48th Annu. Forum Geol. Ind. Miner. (2012).
8. J. William D. Callister, and D. G. Rethwisch, "Materials Science and Engineering: An Introduction 9E," John Wiley Sons, Inc **9** (2014), pp. 266–267.
9. L. Pauling, *The Nature of the Chemical Bond and the Structure of Molecules and Crystals: An Introduction to Modern Structural Chemistry* (1992).
10. H. J. Blankenburg, *Quartzrohstoffe*, VEB Duetscher Verlag fur Grundstoffindustrie (1978).
11. O. W. Florke, "Fortschr.," Mineral (1964).
12. R. B. Sosman, *The Phases of Silica*, Rutgers University Press, New Jersey (1965).
13. D. W. Richerson, *Modern Ceramic Engineering* (1992).
14. R. E. Gibson, "The Influence of Pressure on the High-Low Inversion of Quartz," J. Phys. Chem. **32** (1928), pp. 1197–1205.
15. I. Fanderlik, *Silica Glass and Its Application*, Elsevier Science (1991).
16. J. Chase, M.W., "NIST-JANAF Thermochemical Tables," J. Phys. Chem. Ref. Data, Monogr. 9 **4** (1998), pp. 1-1951 (https://webbook.nist.gov/cgi/cbook.cgi?ID=.
17. D. E. Damby, E. W. Llewellin, C. J. Horwell, B. J. Williamson, J. Najorka, G. Cressey, and M. Carpenter, "The α-β Phase Transition in Volcanic Cristobalite," J. Appl. Crystallogr. **47** (2014), pp. 1205–1215.
18. M. S. Ghiorso, I. S. E. Carmichael, and L. K. Moret, "Inverted High-Temperature Quartz: Unit Cell Parameters and Properties of the α-β Inversion," Contrib. to Mineral. Petrol. **68** (1979), pp. 307–323.
19. W. D. Kingery, H. K. Bowen, and D. R. Uhlmann, *Introduction to Ceramics* (1976).

20. D. L. Lakshtanov, S. V. Sinogeikin, and J. D. Bass, “High-Temperature Phase Transitions and Elasticity of Silica Polymorphs,” Phys. Chem. Miner. **34** (2007), pp. 11–22.
21. F. M. Wahl, R. E. Grim, and R. B. Graf, “Phase Transformations in Silica-Alumina Mixtures as Examined by Continuous x-Ray Diffraction,” Am. Mineral. **45** (1961), pp. 1064–1076.
22. W. A. Deer, R. A. Howie, and J. Zussman, *An Introduction to the Rock-Forming Minerals*, Mineralogical Society of Great Britain and Ireland (2013).
23. A. E. Ghaly, and A. Ergudenler, “Agglomeration of Silica Sand in a Fluidized Bed Gasifier Operating on Wheat Straw,” Agric. Eng. **4** (1993), pp. 135–147.
24. P. Chaivatamaset, P. Sricharoon, S. Tia, and B. Bilitewski, “The Characteristics of Bed Agglomeration/Defluidization in Fluidized Bed Firing Palm Fruit Bunch and Rice Straw,” Appl. Therm. Eng. **70** (2014), pp. 737–747.
25. P. Chaivatamaset, and S. Tia, “The Characteristics of Bed Agglomeration during Fluidized Bed Combustion of Eucalyptus Bark,” Appl. Therm. Eng. **75** (2015), pp. 1134–1146.
26. T. Baumann, and S. Zunft, “Properties of Granular Materials as Heat Transfer and Storage Medium in CSP Application,” Sol. Energy Mater. Sol. Cells **143** (2015), pp. 38–47.